Scientific Research Publishing

Open Journal of Medical Imaging, 2023, 13, 114-126
https://www.scirp.org/journal/ojmi
ISSN Online: 2164-2796
ISSN Print: 2164-2788

Image Non-Uniformity Correction in 3T Gd-EOB-DTPA-Enhanced Magnetic Resonance Imaging: Comparison among Different Software Versions

Hirofumi Hata[1], Yusuke Inoue[2], Keiji Matsunaga[2], Kaoru Fujii[2], Toshio Tamiya[3], Ai Nakajima[1], Yuki Takato[1], Kazuki Hashizume[1*]

[1]Department of Radiology, Kitasato University Hospital, Sagamihara, Japan
[2]Department of Diagnostic Radiology, Kitasato University School of Medicine, Sagamihara, Japan
[3]School of Medicine, Kitasato University, Sagamihara, Japan
Email: *kmri@kitasato-u.ac.jp

How to cite this paper: Hata, H., Inoue, Y., Matsunaga, K., Fujii, K., Tamiya, T., Nakajima, A., Takato, Y. and Hashizume, K. (2023) Image Non-Uniformity Correction in 3T Gd-EOB-DTPA-Enhanced Magnetic Resonance Imaging: Comparison among Different Software Versions. *Open Journal of Medical Imaging*, **13**, 114-126.
https://doi.org/10.4236/ojmi.2023.133012

Received: August 25, 2023
Accepted: September 17, 2023
Published: September 20, 2023

Copyright © 2023 by author(s) and Scientific Research Publishing Inc.
This work is licensed under the Creative Commons Attribution International License (CC BY 4.0).
http://creativecommons.org/licenses/by/4.0/

Open Access

Abstract

Background: Non-uniformity in signal intensity occurs commonly in magnetic resonance (MR) imaging, which may pose substantial problems when using a 3T scanner. Therefore, image non-uniformity correction is usually applied. **Purpose:** To compare the correction effects of the phased-array uniformity enhancement (PURE), a calibration-based image non-uniformity correction method, among three different software versions in 3T Gd-EOB-DTPA-enhanced MR imaging. **Material and Methods:** Hepatobiliary-phase images of a total of 120 patients who underwent Gd-EOB-DTPA-enhanced MR imaging on the same 3T scanner were analyzed retrospectively. Forty patients each were examined using three software versions (DV25, DV25.1, and DV26). The effects of PURE were compared by visual assessment, histogram analysis of liver signal intensity, evaluation of the spatial distribution of correction effects, and evaluation of quantitative indices of liver parenchymal enhancement. **Results:** The visual assessment indicated the highest uniformity of PURE-corrected images for DV26, followed by DV25 and DV25.1. Histogram analysis of corrected images demonstrated significantly larger variations in liver signal for DV25.1 than for the other two versions. Although PURE caused a relative increase in pixel values for central and lateral regions, such effects were weaker for DV25.1 than for the other two versions. In the evaluation of quantitative indices of liver parenchymal enhancement, the liver-to-muscle ratio (LMR) was significantly higher for the corrected images than for the uncorrected images, but the liver-to-spleen ratio (LSR) showed no significant differences.

For corrected images, the LMR was significantly higher for DV25 and DV26 than for DV25.1, but the LSR showed no significant differences among the three versions. **Conclusion:** There were differences in the effects of PURE among the three software versions in 3T Gd-EOB-DTPA-enhanced MR imaging. Even if the non-uniformity correction method has the same brand name, correction effects may differ depending on the software version, and these differences may affect visual and quantitative evaluations.

Keywords

Gd-EOB-DTPA, Non-Uniformity Correction, 3 Tesla, Software Version, Image Contrast

1. Introduction

In magnetic resonance (MR) imaging, spatial variations in radiofrequency transmission and reception cause non-uniformity in the signal intensity, which can pose substantial problems when using a 3T scanner [1] [2] [3]. Therefore, image non-uniformity correction is usually applied. Among the various methods for non-uniformity correction [4] [5] [6], phased-array uniformity enhancement (PURE) is classified as a calibration-based method. Proton density-weighted images are acquired with both the body coil and surface coil to actually measure the sensitivity of the coils [4] [6].

MR imaging with gadolinium-ethoxybenzyl-diethylenetriamine pentaacetic acid (Gd-EOB-DTPA) is widely used to detect focal liver lesions and characterize liver tumors [7] [8]. Gd-EOB-DTPA accumulates in the liver via the organic anion-transporting polypeptide of hepatocytes [9], and aids the detection and characterization of focal liver lesions [7] [8] [9] [10]. Without non-uniformity correction, hyperintensity is observed near the liver surface [11], which may complicate the interpretation of Gd-EOB-DTPA-enhanced MR images. Therefore, non-uniformity correction is required in Gd-EOB-DTPA-enhanced MR imaging. A previous study showed the superiority of PURE over surface coil intensity correction (SCIC) [11], which is an image-based method involving no additional data acquisition [4] [6], for this examination using a 3T scanner. Subsequently, the manufacturer changed the PURE algorithm for the 3T scanner. These changes may have affected image uniformity in 3T Gd-EOB-DTPA-enhanced MR imaging. In this study, we compared three different versions of PURE in 3T Gd-EOB-DTPA-enhanced MR imaging.

2. Materials and Methods

2.1. Subjects

A total of 120 patients who underwent Gd-EOB-DTPA-enhanced MR imaging using the same 3T scanner between April 2015 and August 2019 were included

in the study. We excluded patients with poor breath holding or prior liver resection, and post-splenectomy patients. During the enrollment period, the software version of the scanner was changed from DV25 to DV25.1, and then to DV26. The subjects were comprised of the DV25, DV25.1, and DV26 groups, which included an initial consecutive 20 men and 20 women who were examined using the three corresponding software versions. The study population had a mean ± standard deviation (SD) age of 67.3 ± 9.6 years (68.3 ± 12.6 and 71.5 ± 10.6 years for men and women, respectively). Characteristics of subjects in each group are shown in Table 1.

Table 1. Characteristics of subjects in each group.

Group	Characteristics	Value
DV25	Age (year)	67.3 ± 9.6
	Height (cm)	160.8 ± 9.5
	Weight (kg)	59.5 ± 11.1
	Background liver	
	liver cirrhosis	16
	chronic hepatitis	10
	primary biliary cirrhosis	1
	normal	13
DV25.1	Age (year)	68.3 ± 12.6
	Height (cm)	158.1 ± 9.2
	Weight (kg)	58.1 ± 11.9
	Background liver	
	liver cirrhosis	12
	chronic hepatitis	10
	primary biliary cirrhosis	1
	normal	17
DV26	Age (year)	71.3 ± 10.6
	Height (cm)	160.2 ± 9.6
	Weight (kg)	60.3 ± 12.0
	Background liver	
	liver cirrhosis	19
	chronic hepatitis	9
	primary biliary cirrhosis	2
	normal	10

Means ± SDs are presented for age, height, and weight. The numbers of subjects are shown for background liver.

2.2. Imaging Procedures

MR imaging was performed using a 3T clinical scanner (Discovery 750w; GE Healthcare, Waukesha, WI, USA) with a 32-channel phased-array coil. For dynamic imaging, Gd-EOB-DTPA (0.025 mmol/kg; Bayer Yakuhin, Osaka, Japan) was administered intravenously, and hepatobiliary-phase images were acquired 20 min later using a T1-weighted three-dimensional gradient echo sequence (liver acquisition with volume acceleration [LAVA]). Typical imaging parameters are shown in Table 2. The array spatial sensitivity encoding technique (ASSET) was used with a reduction factor of 2.5. Calibration images were acquired with the body coil and surface coil using a three-dimensional fast spoiled gradient-recalled echo sequence, and the images acquired with the surface coil were used for ASSET reconstruction. The preset mode was used for radiofrequency transmission. Image non-uniformity correction was performed using PURE. Uncorrected and corrected images were stored in a picture archiving and communication system (PACS).

2.3. Visual Assessment of Uniformity

The uniformity of liver signal intensity was visually assessed on a PACS viewer (EV Insite; PSP Corp., Tokyo, Japan) by three board-certified diagnostic radiologists independently. Each image set was randomly displayed on the PACS viewer. The observers were given no information about non-uniformity correction. They reviewed all slices, adjusting the display grayscale according to their preference, and graded superficial hyperintensity, *i.e.*, hyperintensity near the liver surface, as an indicator of non-uniformity, using a three-point scoring system: 1 (severe), 2 (mild), and 3 (negligible). The observers graded each image set using reference images provided to help them understand the scoring system (Figure 1). The visual score for each image set was defined as the mean value of the scores for the three observers.

Table 2. Typical imaging parameters for LAVA sequence.

Parameter	Value
Repetition time (ms)	4.9
Echo time (ms)	1.8
Flip angle (˚)	12
Receiver bandwidth (kHz)	±83.3
Field of view (mm)	360
True spatial resolution (mm^3)	1.1 × 1.9 × 5.0
Reconstructed spatial resolution (mm^3)	0.7 × 0.7 × 2.5
Number of slices	44

The field of view and the number of slices were increased in large patients.

Figure 1. Reference images prepared for visual assessment of superficial hyperintensity near the liver surface: (a) severe (uncorrected image); (b) mild (corrected image); and (c) negligible (corrected image).

2.4. Histogram Analysis of Signal Intensity

Histogram analysis of liver signal intensity was conducted in 20 patients for each group, *i.e.*, the initial consecutive 10 men and 10 women without focal liver lesions > 3 cm. The analysis was performed using a previously described method [11]. A histogram of liver signal intensities for each image set was created using ImageJ software (ver. 1.53e; National Institutes of Health, Bethesda, MD, USA). Seven slices around the level of the porta hepatis were selected so that the axial coordinate of the selected slice was located 1 cm from that of the adjacent selected slice. Regions of interest (ROIs) were drawn manually to cover the entire liver on selected uncorrected image slices and were also applied to the corrected images. A histogram (frequency vs. signal intensity) for a given image set was generated using data from the seven slices, and a simple averaging of 15 consecutive frequency values was performed. The mode signal of the histogram was determined. The signal range including the mode signal and continuously showing frequencies of more than half of the frequency at the mode was determined and the width of this range was divided by the mode signal to define full-width at half-maximum (FWHM). Full-width at quarter-maximum (FWQM) was defined similarly. The FWHM and FWQM were regarded as quantitative indicators of image uniformity, with high values indicating large variations in liver signals and poor uniformity.

2.5. Correction Factors for Non-Uniformity Correction

To evaluate the spatial distribution of the effect of correction, correction maps were created for the same patients included in the histogram analysis, by dividing the corrected image by the uncorrected image at the level of the porta hepatis using ImageJ software. Circular ROIs (1000 mm^2) were placed on the uncorrected image at the center and four peripheral regions (anterior, posterior, right, and left). They were applied to the correction map, and a mean value was obtained for the ROI. The normalized correction factor (nCF) was defined as the mean value of each ROI divided by that of the posterior ROI. In addition, a nCF map was created by dividing the correction map by the mean value of the posterior ROI.

2.6. Quantitative Indices of Liver Parenchymal Enhancement

The liver-to-muscle ratio (LMR) and liver-to-spleen ratio (LSR) of signals were obtained as quantitative indices of liver parenchymal enhancement. ROIs were set on the corrected images and applied to the uncorrected images. For the liver, circular ROIs (100 mm^2) were set in the anterior and posterior segments of the right hepatic lobe and medial segment of the left lobe, avoiding vessels, tumors, and artifacts (Figure 2). Liver signal intensity was defined as the average of the mean signal intensities of the three ROIs. For muscle, circular ROIs (100 mm^2) were set in the right and left paravertebral muscles, while minimizing the inclusion of fat. Muscle signal intensity was defined as the average of the mean signal intensities in the right and left ROIs. A slice showing the right main branch of the portal vein was used to assess liver and muscle signals. Spleen signal intensity was defined as the mean signal intensity in a circular ROI (200 mm^2) set at the splenic hilum level. The LMR and LSR were calculated for each image by dividing the liver signal by the muscle and spleen signals, respectively.

2.7. Statistical Analysis

Values are expressed as means ± SD. Statistical analyses were conducted using R version 4.2.1 (R Foundation for Statistical Computing, Vienna, Austria). Comparisons among patient groups distinguished according to the software version used (independent groups) were performed by one-way analysis of variance (ANOVA) followed by the Tukey-Kramer test for parametric data, and the Kruskal–Wallis test followed by the Steel-Dwass test for nonparametric data. Data with and without non-uniformity correction were compared using the paired t-tests (for parametric data) and the Wilcoxon signed-rank test (nonparametric data). When comparing nCFs among the different ROIs (repeated measures), repeated-measures ANOVA followed by Scheffe's multiple comparisons test was used for parametric data, and the Friedman test followed by the

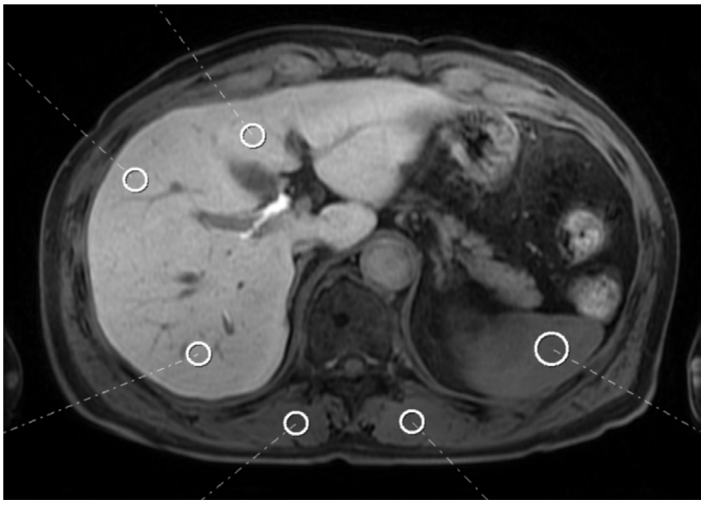

Figure 2. Regions of interest (ROIs) to assess signal intensities in the liver, muscle, and spleen.

Wilcoxon signed-rank test was applied for nonparametric data. In all analyses, $p < 0.05$ was taken to indicate statistical significance. For visual assessment, Fleiss's kappa statistics were calculated to assess interobserver agreement.

3. Result

3.1. Visual Assessment of Uniformity

Severe superficial hyperintensity was observed in most uncorrected image sets, and tended to be evident in the anterior and posterior parts of the liver. The mean visual scores were close to 1 in all three groups, and there were no significant differences among the groups (Figure 3). The visual scores were higher for the corrected than uncorrected images in all groups, indicating improved uniformity of liver signals ($p < 0.05$ for all groups). The score was highest for the DV26 group, followed by the DV25 and DV25.1 groups, and there were significant differences in all paired comparisons ($p < 0.05$ for all comparisons). Fleiss's kappa coefficient was 0.633, showing substantial agreement.

3.2. Histogram Analysis of Signal Intensity

Neither the FWHM nor FWQM differed significantly among the three groups for the uncorrected images (Figure 4). The FWHM and FWQM were smaller for the corrected than uncorrected images in all groups, indicating improved image uniformity ($p < 0.05$ in all groups). The FWHM and FWQM were significantly larger for the DV25.1 group than for the other two groups ($p < 0.05$ in both group comparisons).

3.3. Correction Factors for Non-Uniformity Correction

Examples of nCF maps are presented in Figure 5. The nCF were lower in the peripheral regions than the central region, indicating that PURE decreased peripheral pixel values relative to central values; this corresponds to depression of

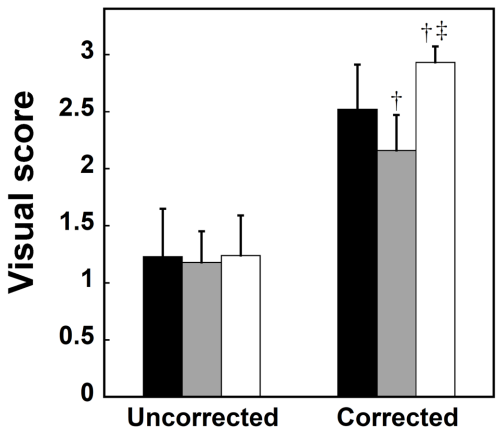

Figure 3. Visual scores. The black, gray, and white columns represent mean values in the DV25, DV25.1, and DV26 groups, respectively. The error bars show SDs. The symbols † and ‡ indicate significant differences compared to the DV25 and DV25.1 groups, respectively.

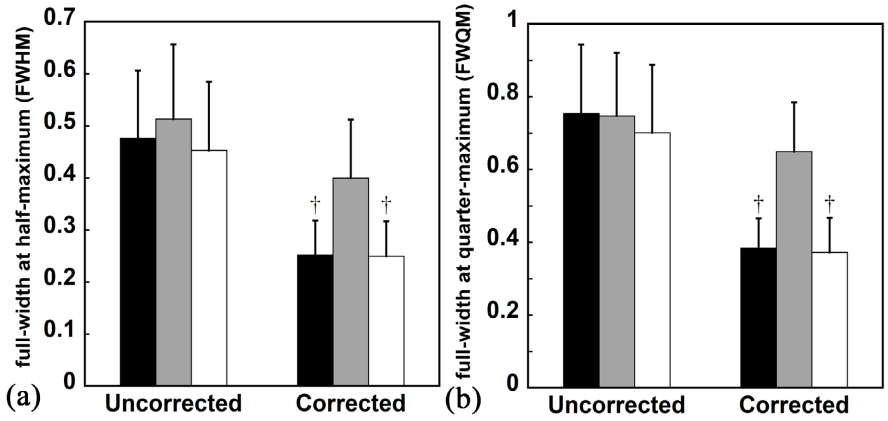

Figure 4. (a) full-width at half-maximum (FWHM) and (b) full-width at quarter-maximum (FWQM) values determined by histogram analysis. The black, gray, and white columns represent mean values in the DV25, DV25.1, and DV26 groups, respectively. The error bars show SDs. The symbol † indicates a significant difference compared to the DV25.1 group.

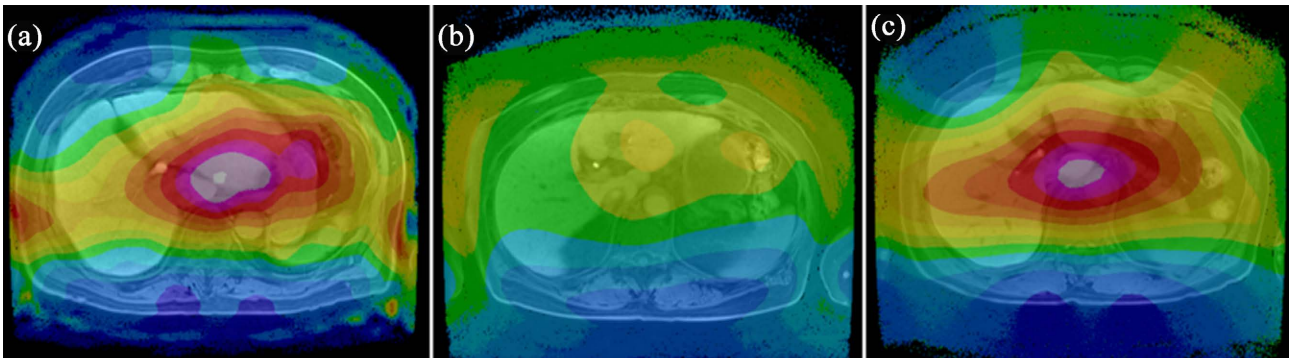

Figure 5. Examples of normalized correction factor (nCF) maps fused with PURE-corrected images in the (a) DV25, (b) DV25.1, and (c) DV26 groups. The nCF maps were displayed using a color scale ranging from 0 to 4.

superficial hyperintensity. The nCF maps in the DV25 and DV26 groups showed lower nCFs in the anterior and posterior regions than in the right and left regions, implying stronger depression of superficial hyperintensity in the anterior and posterior regions. The nCF in the DV25 and DV26 groups were significantly lower for the anterior region than for the right and left regions ($p < 0.05$ in both groups) (**Figure 6**).

The nCF maps demonstrated that the nCFs tended to be lower in the DV25.1 group throughout the image section than in the DV25 and DV26 groups, implying weaker correction effects (**Figure 5**). The nCFs for the right, left, and central regions were significantly lower in the DV25.1 group than the other two groups (**Figure 6**). For the anterior region, the nCF was significantly lower in the DV25.1 than DV26 group, but there was no significant difference between the DV25 and DV25.1 groups (**Figure 6**).

3.4. Quantitative Indices of Liver Parenchymal Enhancement

Neither LMR nor LSR differed significantly among the three groups for the un-

corrected images (Figure 7). Compared with the uncorrected images, the LMR was higher for the corrected images ($p < 0.05$ in all groups). The LMR for the corrected images was significantly higher in the DV25 and DV26 groups than in the DV25.1 group ($p < 0.05$ in both group comparisons). Compared with the uncorrected images, the LSR was higher for the corrected images ($p < 0.05$ in all groups), but there were no significant differences among the three groups.

4. Discussion

The primary purpose of Gd-EOB-DTPA-enhanced MR imaging is to evaluate focal liver lesions [7] [8] [9] [10]. Local non-uniformity of the liver signal may disturb determining an optimal image display, and consequently, evaluating liver lesions. It takes more time for the diagnostic radiologist to adjust the image

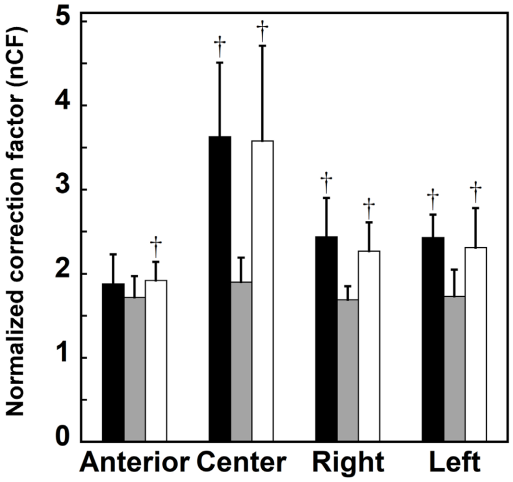

Figure 6. Normalized correction factor (nCFs). The black, gray, and white columns represent mean values for the DV25, DV25.1, and DV26 groups, respectively. The error bars show SDs. The symbol † indicates a significant difference compared to the DV25.1 group.

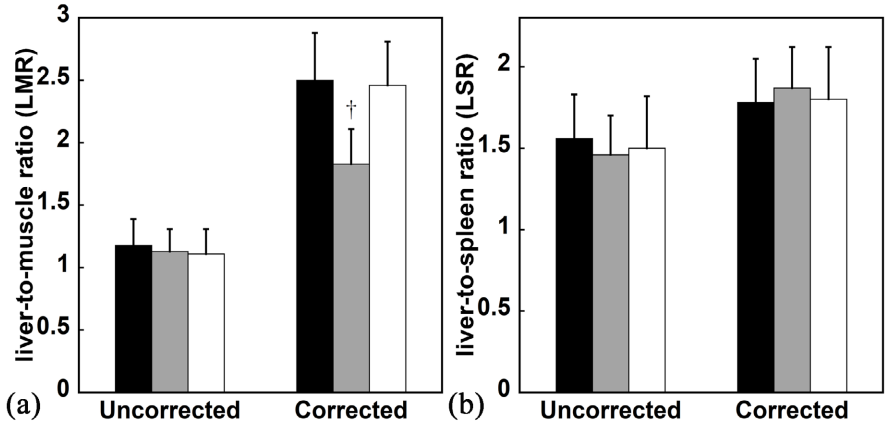

Figure 7. (a) liver-to-muscle ratio (LMR) and (b) liver-to-spleen ratio (LSR). The black, gray, and white columns represent mean values for the DV25, DV25.1, and DV26 groups, respectively. The error bars show SDs. The symbol † indicates significant differences compared to the DV25 and DV26, respectively.

display scale (*i.e.*, window width and window level), which may increase the time required for image reading. A previous study showed that PURE was superior to SCIC for non-uniformity correction in 3T Gd-EOB-DTPA-enhanced MR imaging [11]. PURE is a calibration-based method similar to Prescan Normalize (Siemens) and CLEAR (Philips) provided by other vendors and is commonly used [5]. In this study, we compared the effects of non-uniformity correction among different versions of the PURE method, which was applied to Gd-EOB-DTPA-enhanced hepatobiliary-phase images obtained using a 3T scanner. Although the subjects differed among the software version groups, there were no significant group differences for any indices assessed in the uncorrected images, thus indicating no group differences in the degree of non-uniformity for the uncorrected images. Therefore, the differences in the corrected images among software versions were considered to be due to the differences in the algorithm for each software version.

We performed visual assessments of hyperintensity near the liver surface as an indicator of non-uniformity. Uncorrected images showed superficial hyperintensity near the liver surface. Correction with all software versions of PURE improved the uniformity of the liver signal. However, the degree of improvement differed among software versions, and visual scores were higher in the order of DV26, DV25, and DV25.1. The DV26 version, released last among the three versions, effectively resolved superficial hyperintensity.

Histogram analysis was performed for objective assessment of liver signal non-uniformity. The FWHM and FWQM values for each image set were determined through this analysis. Low FWHM and FWQM values mean that signal variations are small and the uniformity of the liver signal is high [11]. After correcting the data with PURE, the FWHM and FWQM values decreased, implying an improvement in uniformity. The effects of lowering the FWHM and FWQM values were significantly weaker for DV25.1 compared to the other software versions, consistent with the results of the visual assessment.

To investigate the spatial distribution of the effect of non-uniformity correction, a correction factor map was created by dividing the corrected image by the uncorrected image. The correction factor was smallest in the posterior region of the body, which may have been because the coil sensitivity of the MR scanner used in this study was higher in the posterior region than the anterior region. The correction factor normalized to that in the posterior region was higher in the central than the peripheral region, reflecting lower sensitivity in the central region. In DV25.1, the nCF was small, especially in the central and lateral regions, indicating insufficient non-uniformity correction.

The LSR and LMR are widely used as simple quantitative indices of liver parenchymal enhancement in Gd-EOB-DTPA-enhanced MR imaging [7] [12] [13] [14] [15] [16]. The LMR and LSR represent the liver signal normalized to the muscle and spleen signals, respectively [13] [14] [15]. However, it has been pointed out that such indices derived from hepatobiliary-phase images only may be affected by differences in scanners and scan parameters [7] [12] [16]. In this

study, the effects of differences in software versions for non-uniformity correction were assessed using the same scanner and scan parameters. Non-uniformity correction using PURE increased the LMR, which may have been because the ROIs for the liver were located more deeply than those for the muscle and the signal increase due to non-uniformity correction was stronger for the liver. The LSR was also increased by PURE, but the degree was mild. This may have been because the difference in depth between the liver and spleen ROIs was small. After non-uniformity correction, the LMR showed significant differences among software versions and was significantly lower for DV25.1 than for the other software versions. In Gd-EOB-DTPA-enhanced MR imaging using a 3T scanner, it should be noted that the quantitative indices of liver parenchymal enhancement may differ depending on the software version used, even when non-uniformmity correction of the same brand name is applied. The LMR is particularly susceptible to non-uniformity correction.

We found that PURE improved uniformity irrespective of the version; however, the degree of improvement differed among versions, which affected the quantitative indices of liver parenchymal enhancement. When the software version of the MR scanner is changed, it is necessary to check whether the algorithm for non-uniformity correction has also been changed. In addition, studies regarding Gd-EOB-DTPA-enhance MR imaging using a 3T scanner must clarify the software version used for non-uniformity correction rather than simply reporting that PURE was used.

This study had some limitations. First, the three software versions were applied to different patients. Although no differences in uncorrected images were observed, intra-patient comparisons are desirable. We evaluated non-uniformity correction provided by a single manufacturer; further studies involving other manufacturers are required. In addition, the effects of differences in a non-uniformity correction on diagnostic performance, and the efficiency of Gd-EOB-DTPA-enhanced MR image reading, remain to be examined in future investigations.

5. Conclusion

We compared three different software versions of PURE in 3T Gd-EOB-DTPA-enhanced MR imaging and demonstrated differences in correction effects. Even if the non-uniformity correction method has the same brand name, correction effects may differ depending on the software version, and these differences may affect visual and quantitative evaluations.

Acknowledgements

The authors would like to thank Mr. Hiroki Miyatake for his support in the statistical analysis.

Funding

This research received no specific grant from any funding agency in the public,

commercial, or not-for-profit sectors.

Conflicts of Interest

The authors declare no conflicts of interest regarding the publication of this paper.

References

[1] Bernstein, M.A., Huston 3rd, J. and Ward, H.A. (2006) Imaging Artifacts at 3.0T. Journal of *Magnetic Resonance Imaging*, **24**, 735-746. https://doi.org/10.1002/jmri.20698

[2] Soher, B.J., Dale, B.M. and Merkle, E.M. (2007) A Review of MR Physics: 3T versus 1.5T. *Magnetic Resonance Imaging Clinics of North America*, **15**, 277-290. https://doi.org/10.1016/j.mric.2007.06.002

[3] Dietrich, O., Reiser, M.F. and Schoenberg, S.O. (2008) Artifacts in 3-T MRI: Physical Background and Reduction Strategies. *European Journal of Radiology*, **65**, 29-35. https://doi.org/10.1016/j.ejrad.2007.11.005

[4] Liney, G.P., Owen, S.C., Beaumont, A.K.E., Lazar, V.R., Manton, D.J. and Beavis, A.W. (2013) Commissioning of a New Wide-Bore MRI Scanner for Radiotherapy Planning of Head and Neck Cancer. *British Journal of Radiology*, **86**, Article ID: 20130150. https://doi.org/10.1259/bjr.20130150

[5] Thomas, M.S., Greenwood, R., Nolan, C., Malcolm, P.N. and Toms, A.P. (2014) Optimizing MRI of Small Joints and Extremities. *Clinical Radiology*, **69**, e414-e421. https://doi.org/10.1016/j.crad.2014.06.002

[6] Felemban, D., Verdonschot, R.G., Iwamoto, Y., Uchiyama, Y., Kakimoto, N., Kreiborg, S. and Murakami, S. (2018) A Quantitative Experimental Phantom Study on MRI Image Uniformity. *Dentomaxillofacial Radiology*, **47**, Article ID: 20180077. https://doi.org/10.1259/dmfr.20180077

[7] Murakami, T., Sofue, K. and Hori, M. (2022) Diagnosis of Hepatocellular Carcinoma Using Gd-EOB-DTPA MR Imaging. *Magnetic Resonance in Medical Sciences*, **21**, 168-181. https://doi.org/10.2463/mrms.rev.2021-0031

[8] Li, X-Q., Wang, X., Zhao, D-W., Sun, J., Liu, J-J., Lin, D-D., Yang, G., Liu, H., Xia, Z-Y., Jia, C-Y. and Li, H-J. (2020) Application of Gd-EOB-DTPA-Enhanced Magnetic Resonance Imaging (MRI) in Hepatocellular Carcinoma. *World Journal of Surgical Oncology*, **18**, Article No. 219. https://doi.org/10.1186/s12957-020-01996-4

[9] Van Beers, B.E., Pastor, C.M. and Hussain, H.K. (2012) Primovist, Eovist: What to Expect? *Journal of Hepatology*, **57**, 421-429. https://doi.org/10.1016/j.jhep.2012.01.031

[10] Inchingo, R., Faletti, R., Grazioli, L., Tricario, E., Gatti, M., Pecorelli, A. and Ippolito, D. (2018) MR with Gd-EOB-DTPA in Assessment of Liver Nodules in Cirrhotic Patients. *World Journal of Hepatology*, **10**, 462-473. https://doi.org/10.4254/wjh.v10.i7.462

[11] Ogasawara, G., Inoue, Y., Matsunaga, K., Fujii, K., Hata, H. and Takato, Y. (2017) Image Non-Uniformity Correction for 3-T Gd-EOB-DTPA-Enhanced MR Imaging of the Liver. *Magnetic Resonance in Medical Sciences*, **16**, 115-122. https://doi.org/10.2463/mrms.mp.2016-0012

[12] Bae, K.E., Kim, S.Y., Lee, S.S., Kim, K.W., Won, H.J., Shin, Y.M., Kim, P.N. and Lee, M-G. (2012) Assessment of Hepatic Function with Gd-EOB-DTPA-Enhanced Hepatic MRI. *Digestive Diseases*, **30**, 617-622. https://doi.org/10.1159/000343092

[13] Poetter‐Lang, S., Bastati, N., Messner, A., Kristic, A., Heroid, A., Hodge, J.C. and Ba-Ssalamah, A. (2020) Quantification of Liver Function Using Gadoxetic Acid-Enhanced MRI. *Abdominal Radiology*, **45**, 3532-3544. https://doi.org/10.1007/s00261-020-02779-x

[14] Bártulos, C.R., Senk, K., Schumacher, M., Plath, J., Kaiser, N., Bade, R., Woetzel, J. and Wiggermann, P. (2022) Assessment of Liver Function with MRI: Where Do We Stand? *Frontiers in Medicine*, **9**, Article 839919. https://doi.org/10.3389/fmed.2022.839919

[15] Ai, X., Wang, H., Yang, Y., Feng, Y., Xie, X., Zhao, X., Li, J., Yao, P. and Zhu, Q. (2023) Four Indices on Gd-EOB-DTPA-Enhanced MRI Can Estimate Liver Functional Reserve Compared to ICG-R15: A Systematic Review and Meta-Analysis. *Clinical Imaging*, **102**, 1-8. https://doi.org/10.1016/j.clinimag.2023.06.018

[16] Mori, H. and Akimoto, S. (2022) Liver-Spleen Contrast Standardization of Gadolinium-Ethoxybenzyl-Diethylenetriamine Penta-Acetic Acid-Enhanced Magnetic Resonance Imaging Based on Cross-Calibration. *Quantitative Imaging in Medicine and Surgery*, **12**, 5343-5357. https://doi.org/10.21037/qims-22-174